
Biodistribution and Pharmacokinetics of the $\alpha_v\beta_3$ -Selective Tracer ^{18}F -Galacto-RGD in Cancer Patients

Ambros J. Beer, MD^{1,2}; Roland Haubner, PhD¹; Michael Goebel, MD³; Stephan Luderschmidt, MD⁴; Mary E. Spilker, PhD¹; Hans-Jürgen Wester, PhD¹; Wolfgang A. Weber, MD¹; and Markus Schwaiger, MD¹

¹Department of Nuclear Medicine, Technische Universität München, Munich, Germany; ²Department of Radiology, Technische Universität München, Munich, Germany; ³Department of Orthopedic Surgery, Technische Universität München, Munich, Germany; and ⁴Department of Dermatology, Technische Universität München, Munich, Germany

^{18}F -Galacto-RGD has been developed for PET of $\alpha_v\beta_3$ integrin expression, a receptor involved in, for example, angiogenesis and metastasis. Our aim was to study the kinetics and biodistribution of ^{18}F -Galacto-RGD in cancer patients. **Methods:** Nineteen patients with metastases of malignant melanoma ($n = 7$), sarcomas ($n = 10$), or osseous metastases ($n = 2$) were examined. After injection of 133–200 MBq ^{18}F -Galacto-RGD, 3 consecutive emission scans from the pelvis to the thorax or dynamic emission scans of the tumor over 60 min, followed by 1 static emission scan of the body, were acquired. Time–activity curves and standardized uptake values (SUVs) were derived by image region-of-interest analysis with image-based arterial input functions. Compartmental modeling was used to derive the distribution volume for muscle tissue and tumors. **Results:** ^{18}F -Galacto-RGD showed rapid blood clearance and primarily renal excretion. SUVs in tumors ranged from 1.2 to 9.0. Tumor-to-blood and tumor-to-muscle ratios increased over time, with peak ratios of 3.1 ± 2.0 and 7.7 ± 4.3 , respectively, at 72 min. The tumor kinetics were consistent with a 2-tissue compartment model with reversible specific binding. Distribution volume values were, on average, 4 times higher for tumor tissue (1.5 ± 0.8) than those for muscle tissue (0.4 ± 0.1). The data suggest that there was only minimal free and bound (specific or nonspecific) tracer in muscle tissue. **Conclusion:** ^{18}F -Galacto-RGD demonstrates a highly favorable biodistribution in humans with specific receptor binding. Most important, this study shows that ^{18}F -Galacto-RGD allows visualization of $\alpha_v\beta_3$ expression in tumors with high contrast. Consequently, this tracer offers a new strategy for noninvasive monitoring of molecular processes and may supply helpful information for planning and controlling of therapeutic approaches targeting the $\alpha_v\beta_3$ integrin.

Key Words: ^{18}F -Galacto-RGD; $\alpha_v\beta_3$ expression; PET; whole-body biodistribution; kinetic modeling

J Nucl Med 2005; 46:1333–1341

Received Feb. 10, 2005; revision accepted Apr. 19, 2005.
For correspondence contact: Ambros J. Beer, MD, Department of Nuclear Medicine, Technische Universität München, Klinikum rechts der Isar, Ismaninger Strasse 22, 81675 Munich, Germany.
E-mail: beer@roe.med.tum.de

Integrins are heterodimeric glycoproteins, which are involved in cell–cell and cell–matrix interactions (1). One member of this class of receptors is the integrin $\alpha_v\beta_3$, which has been shown to play an essential role in the regulation of tumor growth, local invasiveness, and metastatic potential (2,3). Moreover, $\alpha_v\beta_3$ is also highly expressed on activated endothelial cells during angiogenesis (4). Inhibition of the $\alpha_v\beta_3$ -mediated cell–matrix interactions has been found to induce apoptosis of activated endothelial cells. However, $\alpha_v\beta_3$ antagonists can induce apoptosis not only of endothelial cells but also of $\alpha_v\beta_3$ -positive tumor cells, resulting in a direct cytotoxic effect on these cells (5). Thus, the use of $\alpha_v\beta_3$ antagonists is currently being evaluated as a strategy for anticancer therapy (6). However, currently available morphologic imaging techniques such as CT or MRI are limited in monitoring treatment with this new class of drugs. The response rate and success of an antitumor therapy are generally assessed by evidence of a significant reduction of the tumor size achieved during therapy. Yet, this method may not be applicable for a therapy with $\alpha_v\beta_3$ antagonists, which is aimed at disease stabilization and prevention of metastases. Therefore, noninvasive determination of $\alpha_v\beta_3$ expression would be crucial for the assessment of receptor expression during therapy and for the pretherapeutic recognition of those patients most amenable to $\alpha_v\beta_3$ -directed therapies.

Several integrins, including $\alpha_v\beta_3$, bind to the tripeptide sequence arginine-glycine-aspartic acid (single-letter code RGD) of different matrix proteins, such as fibronectin and vitronectin (7). On the basis of the $\alpha_v\beta_3$ -selective pentapeptide cyclo(-Arg-Gly-Asp-D-Phe-Val-), a variety of radiolabeled $\alpha_v\beta_3$ antagonists for SPECT and PET have been developed (8). The glycosylated cyclic pentapeptide ^{18}F -Galacto-RGD resulted from tracer optimization based on the first-generation peptide ^{125}I -3-iodo-D-Tyr⁴-cyclo(-Arg-Gly-Asp-D-Tyr-Val-) (9). ^{18}F -Galacto-RGD demonstrated high affinity and selectivity for the $\alpha_v\beta_3$ integrin in vitro, receptor-specific accumulation in a murine $\alpha_v\beta_3$ -positive

tumor model, as well as high metabolic stability and predominantly renal elimination (10,11). Moreover, initial data from our patient study indicate that this tracer can be used to noninvasively determine $\alpha_v\beta_3$ expression in humans (12,13). The present study was performed for detailed characterization of the biodistribution and pharmacokinetics of ^{18}F -Galacto-RGD in cancer patients. Patients with melanomas and musculoskeletal sarcomas have been chosen, because the role of $\alpha_v\beta_3$ in angiogenesis and metastatic potential has already been described for these tumors (10,14). Moreover, phase I and phase II studies with humanized anti- $\alpha_v\beta_3$ antibodies have already been performed in patients with soft-tissue sarcomas (15,16).

MATERIALS AND METHODS

Radiopharmaceutical Preparation

Synthesis of the labeling precursor and subsequent ^{18}F labeling were performed as described previously (11). For application in patients, high-performance liquid chromatography eluent was completely removed by evaporation, and 0.5 mL absolute ethanol and 10 mL phosphate-buffered saline (pH 7.4) were added and passed through a Millex GV filter (Millipore GmbH) before injection.

Patients

The study was approved by the ethics committee of the Technische Universität München and informed written consent was obtained from all patients. Nineteen patients included in the study (10 women, 9 men; mean age \pm SD, 55.7 ± 16.2 y; range, 26–89 y), had either malignant melanoma with lymph node or organ metastases ($n = 7$) or malignant lesions of the musculoskeletal system ($n = 12$; Table 1). Inclusion criteria consisted of known or

suspected malignancy, >18 y of age, and the ability to give written and informed consent. Exclusion criteria consisted of pregnancy, lactation period, and impaired renal function (serum creatinine level, >1.2 mg/dL).

PET Procedure

Imaging was performed with either an ECAT EXACT HR+ ($n = 8$) or an ECAT EXACT ($n = 11$) PET scanner (CTI/Siemens). Before tracer injection of ^{18}F -Galacto-RGD (133–200 MBq), a transmission scan was acquired for 5 min per bed position (5 bed positions) using 3 rotating ^{68}Ge rod sources (each with ~ 90 MBq ^{68}Ge). Two imaging protocols were used to study the whole-body distribution and time course of tumor activity. In 6 patients, dynamic emission scans of 22 frames, during 60 min after bolus injection of the tracer, were acquired covering the region of the tumor to obtain time-activity curves in malignant lesions (10 frames \times 30 s, 4 frames \times 60 s, 4 frames \times 180 s, and 4 frames \times 600 s). The dynamic scan was followed by a static emission scan (5 bed positions, 5 min per bed position) covering a field of view from the pelvis to the upper thorax and, when necessary, an additional bed position covering the region of the tumor (when located outside the torso). In the remaining 12 subjects, 3 consecutive static emission scans were acquired in the caudocranial direction, beginning 5 min after injection of ^{18}F -Galacto-RGD, covering a field of view from the pelvis to the thorax (5–7 bed positions, 5 min per bed position). The average starting times of these scans were 6.3 ± 2.7 , 35.7 ± 7.9 , and 72.0 ± 12.2 min (mean \pm SD) after injection.

Image Analysis of Biodistribution Data

Positron emission data were reconstructed using the ordered-subsets expectation maximization (OSEM) algorithm. The OSEM reconstructions were performed with 8 iterations and 4 subsets. The images were attenuation corrected using the transmission data

TABLE 1
Demographics, Pathology, and Scan Protocols of Study Population

Patient no.	Age (y)	Sex	Injected dose (mCi/MBq)	Scan protocol*	Pathology
1	56	M	3.9/144.3	3 ES	Malignant melanoma, stage III (metastases to liver, gut, skin, lymph nodes)
2	89	F	3.9/144.3	3 ES	Malignant melanoma, stage III (metastases to skin)
3	59	F	5.1/188.7	3 ES	Malignant melanoma, stage III (metastases to lymph nodes, lung)
4	44	M	5.4/199.8	3 ES	Malignant melanoma, stage II (metastasis to lymph nodes)
5	36	F	4.2/155.4	3 ES	Malignant melanoma, stage II (metastasis to lymph nodes)
6	76	F	4.5/166.5	1 DS, 1 ES	Malignant melanoma, stage II (metastasis to lymph nodes)
7	66	M	4.4/161.3	1 DS, 1 ES	Malignant melanoma, stage II (metastasis to skin)
8	75	F	4.0/148.0	1 ES	Soft-tissue sarcoma (metastases to lung, bone)
9	26	F	3.7/136.9	3 ES	Chondrosarcoma, grade III, right pelvis
10	74	M	3.6/133.2	1 DS, 1 ES	Malignant fibrous histiocytoma, left thigh
11	57	M	5.3/196.1	1 DS, 1 ES	Chondrosarcoma, grade I, right glenoid
12	35	F	4.7/172.1	3 ES	Osteosarcoma, left distal femur
13	51	M	4.7/172.1	3 ES	Liposarcoma, right thigh
14	41	F	5.1/188.7	3 ES	Osteosarcoma, right proximal fibula
15	42	F	3.9/144.3	1 DS, 1 ES	Chondrosarcoma, grade I, right scapula
16	56	M	5.0/185.0	1 DS, 1 ES	Malignant fibrous histiocytoma, left lower leg
17	55	M	4.1/151.7	3 ES	Osseous metastasis, right proximal femur from renal cell carcinoma
18	65	M	5.1/188.7	3 ES	Osseous metastasis, right pelvis from cholangiocarcinoma
19	84	F	4.8/177.6	3 ES	Liposarcoma, left forearm

*ES = static emission scan of thorax and abdomen (25–30 min); DS = dynamic emission scan (60 min).

collected over the same region of emission imaging. For image analysis, CAPP software, version 7.1 (CTI/Siemens), was used. Images were calibrated to standardized uptake values (SUVs) or to Bq/mL. The SUV was calculated according to the following formula: (measured activity concentration [Bq/mL] \times body weight [g])/injected activity (Bq) (17).

In the static emission scans, circular regions of interest (ROIs) were placed over major organs (lung, left ventricle, liver, spleen, intestine, kidneys, bladder, muscle) and tumor tissue by an experienced operator using the first emission scan acquired shortly after injection. The location of the ROIs was then copied to the second and third emission scans. The diameter of the ROIs was set to 1.5 cm, except for the kidneys and intestine. Here, polygonal ROIs adapted to the contour of the kidney or covering the area of intestine with the maximum activity were drawn. Results are either expressed in SUV or in percentage of the injected dose/volume (%ID/L). The total fraction of injected activity found in the bladder was determined by multiplying the injected dose/volume found in the bladder by the total bladder volume in the last emission scan. The bladder volume was measured by drawing polygonal ROIs around the bladder on each slice with visible bladder activity. For drawing these ROIs, the images were scaled to the maximum SUV in the bladder to avoid an overestimation of the volume due to the high activity concentration in the urine.

Kinetic Modeling

The selection of time–activity curves and subsequent kinetic analyses were performed using the PMOD Medical Imaging Program, version 2.5 (PMOD Group). An ROI approach was applied to the dynamic images to obtain time–activity curves for lesions as well as background tissue (muscle). In the case of tumor tissue, circular ROIs with a diameter of 1.0 cm were drawn over the region with the maximum count density (“tumor maximum”) and in the 2 immediately adjacent slices (18). Additionally, polygonal ROIs were drawn over the whole tumor in all slices with visible tumor uptake. Circular ROIs with a diameter of 15 mm were drawn over muscle tissue in the whole volume of interest. The last frame of the dynamic image series was used to define the ROIs for the tumor, tumor maximum, and muscle. To derive an image-based input function, circular ROIs with a diameter of 5–8 mm were placed over the largest artery in the volume in every slice where the artery could be identified on the frames acquired from 30 to 60 s after injection. All ROIs were then projected onto the complete dynamic dataset and time–activity curves were subsequently derived.

In 2 patients, no correct arterial input function could be derived from the datasets, because the tumors were located below the knee and no adequate artery could be visualized in the scans. Therefore, these scans had to be excluded from the kinetic modeling analysis.

Various compartment models were fitted to the data (Fig. 1) and kinetic constants were estimated by minimizing the sum of squared differences between the tissue time–activity curves and the model-predicted curves. A 2-tissue-compartment (2-TC) model best characterized the tumor and tumor maximum data. In muscle tissue, it was difficult to resolve the second compartment; therefore, a 1-tissue-compartment (1-TC) model was used for further analysis of this tissue. The total distribution volume (DV_{tot}) was calculated for all ROIs based on the directly estimated kinetic rate constants (K_1 – k_4). The peak plasma activity of the tracer might be underestimated by using an image-based arterial input function instead of arterial sampling and, consequently, K_1 might be overestimated

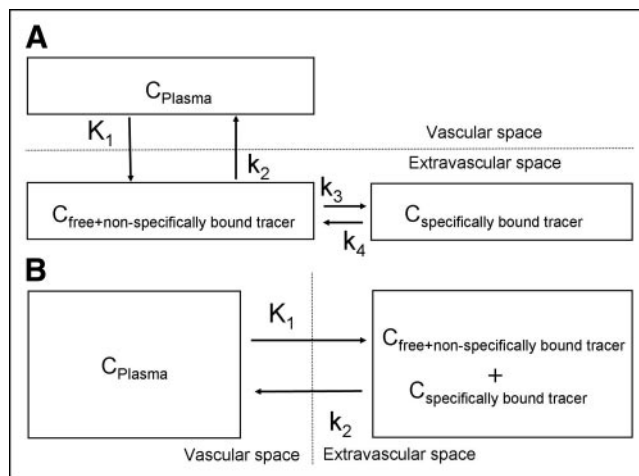


FIGURE 1. Compartmental models used for ^{18}F -Galacto-RGD kinetics. Vascular compartment represents concentration of unmetabolized tracer in plasma (C_{Plasma}). 2-Tissue-compartment model (A) considers 2 extravascular compartments accounting for free and nonspecifically bound tracer in tissue ($C_{\text{free+non-specifically bound tracer}}$) and ^{18}F -Galacto-RGD specifically bound to $\alpha_v\beta_3$ receptors ($C_{\text{specifically bound tracer}}$). In 1-tissue-compartment model (B), all tissue compartments are united to 1 compartment ($C_{\text{free+non-specifically bound tracer}} + C_{\text{specifically bound tracer}}$). K_1 – k_4 = kinetic rate constants.

in our model. Therefore, we also calculated DV_{tot} with K_1 set to 0.1 for comparison, which was 3–4 times lower than the calculated K_1 values. This value was chosen according to results of kinetic modeling studies using ^{18}F -FDG in solid malignant tumors (19). A more-detailed description of the compartment models and the mathematic definition of DV_{tot} can be found elsewhere (20,21).

The half-time of tracer activity in blood was calculated by fitting a biexponential function to the time points after the peak intensity of the time–activity curve derived from the image-based arterial input function.

RESULTS

Figure 2 shows the tracer kinetics of ^{18}F -Galacto-RGD in various organs (mean values of the 12 patients who received 3 emissions scans). Table 2 summarizes the results of the last emission scan of all patients, including the 6 patients who had a dynamic emission scan during the first 60 min and a patient with only 1 static emission scan. ^{18}F -Galacto-RGD shows rapid renal excretion and clearance from the blood pool, with 1.8 %ID/L blood-pool activity 72 min after injection (SUV, 1.3 ± 0.4) and 102 %ID/L urinary bladder activity (SUV, 76.5 ± 38.6). The mean fraction of injected activity found in the bladder at 72 min after injection was $49.2\% \pm 29.1\%$. The dynamic scans revealed a biexponential clearance of tracer activity from the blood with a rapid first half-time of 0.36 ± 0.28 min and a slower second half-time of 34.13 ± 17.15 min.

The highest SUVs in solid organs 72 min after injection were found in the kidneys (SUV, 5.2 ± 3.2), followed by the liver (SUV, 2.7 ± 0.7) and the spleen (SUV, 2.5 ± 0.5). In the liver, there is some retention of activity over time. In

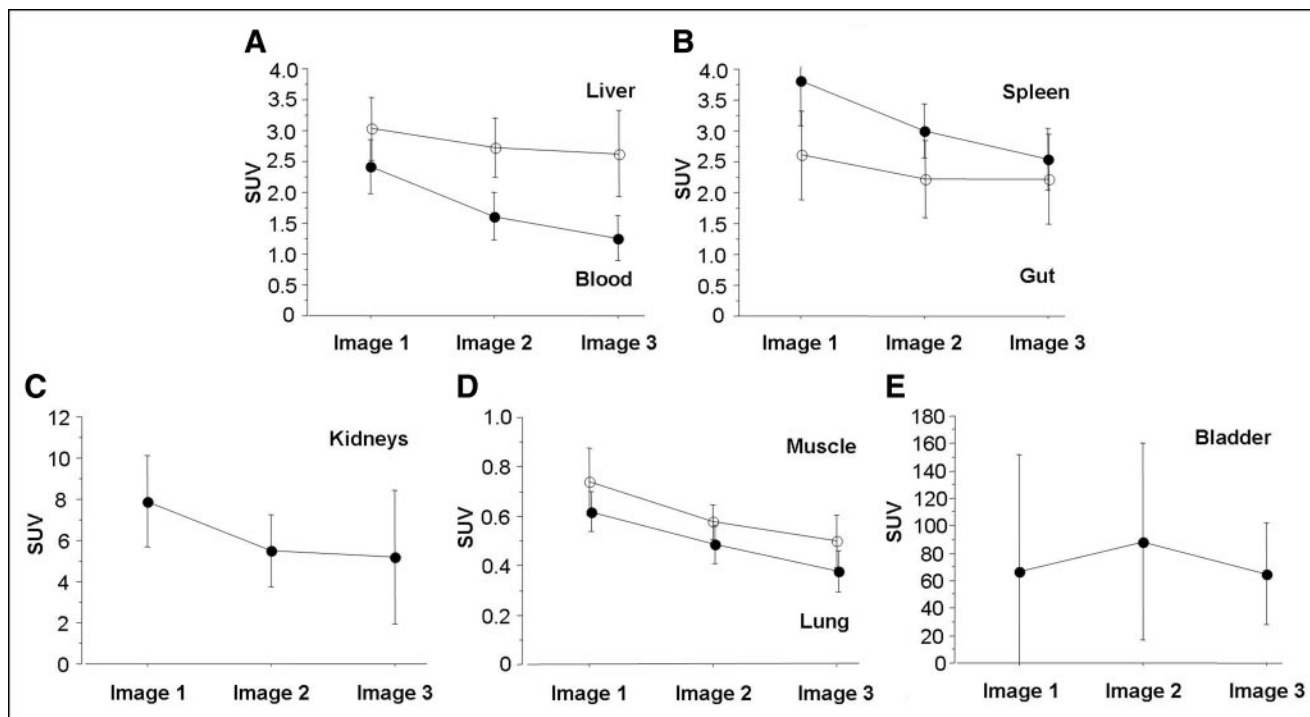


FIGURE 2. Mean SUVs \pm SDs for major organs and muscle tissue on basis of 3 static emission scans of 12 patients (mean start times of acquisition: bladder, 6, 36, and 72 min after injection; intestine, 13, 43, and 79 min after injection; kidneys, 19, 49, and 85 min after injection; liver/spleen, 21, 51, and 87 min after injection; blood [left ventricle]/muscle, 24, 54, and 90 min after injection; lung [apex], 29, 59, and 95 min after injection).

contrast, in the spleen, a rapid decrease of activity over time was found, paralleling the decrease in blood-pool activity. There was no significant tracer accumulation in the gut during the examination period. Low activities in the lung and muscle were found with SUVs of 0.4 ± 0.08 and 0.5 ± 0.1 , respectively.

Tracer uptake in tumor lesions was very heterogeneous. In 17 of 19 (89.4%) patients, 23 of 29 (79.3%) malignant lesions could be detected. In 2 patients, no regionally increased tracer uptake compared with background activity

was found (patients 1 and 19). For 1 patient, the primary tumor as well as an osseous metastasis showed intense tracer uptake, whereas in several pulmonary metastases no tracer uptake was found (patient 8). For another patient, tracer uptake in the primary tumor was moderate, whereas an osseous metastasis showed intense tracer uptake (patient 18). This considerable inter- as well as intraindividual variance in tracer accumulation is reflected in the large SD of the mean SUV for all lesions (Fig. 3). The mean tumor SUV declined only slightly over time to 3.7 ± 2.3 at 72 min after

TABLE 2
Mean SUVs and %ID/L on Basis of Last Emission Scan 72 Minutes After Injection

Parameter	Mean SUV* \pm SD	Minimum	Maximum	Mean %ID/L \pm SD
Blood	1.246 \pm 0.367	0.836	2.206	1.813 \pm 0.604
Liver	2.695 \pm 0.621	1.821	4.071	3.749 \pm 0.836
Spleen	2.657 \pm 0.591	1.640	4.328	3.742 \pm 0.949
Kidneys	5.809 \pm 4.369	3.000	20.065	8.059 \pm 5.394
Gut	2.415 \pm 1.446	1.160	7.661	3.401 \pm 1.803
Muscle	0.470 \pm 0.092	0.361	0.706	0.695 \pm 0.185
Mamma	1.484 \pm 0.127	1.337	1.562	2.410 \pm 0.493
Lung	0.427 \pm 0.071	0.277	0.496	0.564 \pm 0.144
Bladder	76.531 \pm 38.555	24.850	126.100	102.347 \pm 52.364
Tumor	3.688 \pm 2.255	0.804	9.800	5.060 \pm 3.616
Tumor/blood ratio	3.326 \pm 2.236	0.664	9.969	—
Tumor/muscle ratio	7.704 \pm 5.370	1.154	24.747	—

*Data are from last static emission scan at 72 min after injection from all 19 patients.

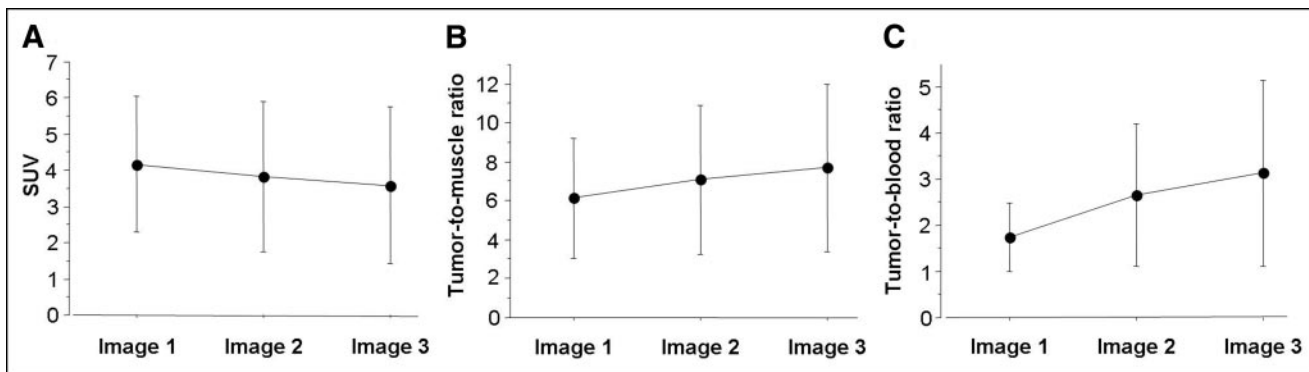


FIGURE 3. Mean SUVs \pm SD in tumors (A), mean tumor-to-muscle ratios \pm SD (B), and mean tumor-to-blood-ratios \pm SD (C) for all tumor lesions with visible uptake (12 lesions in 10 patients (mean start times of acquisition: 6, 36, and 72 min after injection; mean start times of acquisition of tumor regions, 17, 47, and 83 min after injection).

injection, whereas the tumor-to-blood ratio and the tumor-to-muscle ratio increased over time (peak values 3.3 ± 2.2 and 7.7 ± 5.4 , respectively).

In all dynamic scans, tumors showed rapid tracer accumulation during the first 10 min followed by a plateau phase with no, or only minimal, decrease of the activity until 60 min after injection (Fig. 4). The results of the modeling data are summarized in Table 3. The 2-TC model used for tumors and tumor maximum fit well with parameter coefficients of variation (CoV) between 12.3% and 29.3% for tumors and of 24.6%–37.1% for tumor maximum. For muscle, the 1-TC model fits the data best and resulted in parameter CoV values between 15.4% and 16.2%. DV_{tot} values for tumors were always higher than the DV_{tot} for muscle, with a mean ratio of 3.85 for tumors and 9.22 for tumor maximum relative to muscle tissue. Because K_1

might be overestimated by using an image-based input function, we also calculated a model fit with a lower K_1 value of 0.1 for the datasets. In this scenario, the 1-TC model fit better for 3 of 4 patients for tumors and tumor maximum. However, the resulting DV_{tot} values were similar to the results with a calculated K_1 (tumor, 1.41 ± 0.55 ; tumor maximum, 3.60 ± 2.29 ; muscle, 0.37 ± 0.12).

Figure 5 shows representative dynamic coronal image sets of normal organs of emission images acquired at 5, 30, and 60 min after tracer injection. Figure 6 shows a representative example of a patient with a large chondrosarcoma of the pelvis and intense heterogeneous tracer uptake of the tumor, which decreased only slightly over time.

DISCUSSION

In this study, we describe the detailed biodistribution and kinetics of the $\alpha_v\beta_3$ -selective tracer ^{18}F -Galacto-RGD in cancer patients. This tracer shows a predominantly renal excretion with rapid blood clearance allowing imaging of tumor lesions with good contrast. The kinetic modeling data indicate specific receptor binding of ^{18}F -Galacto-RGD with low binding in background tissue. These findings suggest that ^{18}F -Galacto-RGD can be effectively used for imaging of $\alpha_v\beta_3$ expression in humans.

In contrast to the high-activity concentration found in the bladder due to the renal elimination, no increase in activity in the gut was observed, indicating that there is no significant biliary excretion of the tracer into the intestine during the observation period of ~ 90 min. The background activity in muscle tissue and blood pool was very low. However, delineation of lesions with moderate tracer uptake might be impaired in the liver and spleen due to the relatively high background activity in these organs. Image quality in the pelvis might also be impaired by artifacts due to the high bladder activity. However, activity concentration in the bladder can be reduced by administration of a diuretic agent (e.g., furosemide, 20 mg intravenously) together with the tracer similar to protocols used for imaging with ^{18}F -FDG.

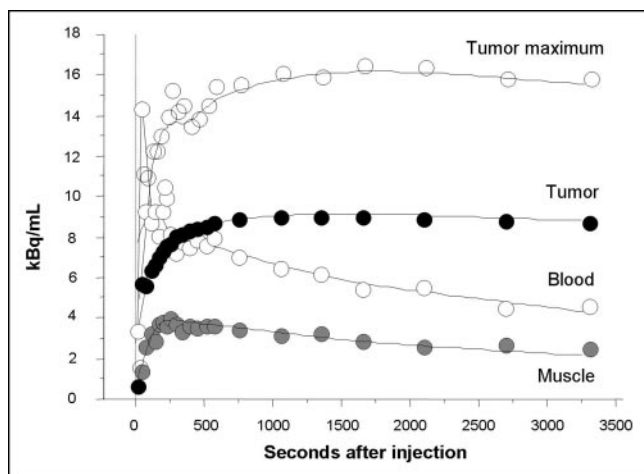


FIGURE 4. Time-activity curves of representative dynamic scan over 60 min (patient 10) for tumor, tumor maximum, and muscle tissue. Circles denote measured data (kBq/mL), whereas lines are results of curve fit of kinetic modeling data, using a 2-TC model for tumor and tumor maximum and a 1-TC model for muscle. Note excellent fit of curves and measured data. The blood curve shows rapid tracer elimination from the blood pool.

TABLE 3
Kinetic Modeling Data

Parameter	Tumor (2-TC)	Tumor maximum (2-TC)	Muscle (1-TC)
K_1	0.436 ± 0.286	1.705 ± 1.160	0.251 ± 0.212
CoV K_1	12.286 ± 2.255	24.556 ± 12.286	15.401 ± 9.892
k_2	1.040 ± 0.958	3.142 ± 4.219	0.665 ± 0.532
CoV k_2	16.347 ± 6.612	34.761 ± 5.634	16.242 ± 18.505
k_3	0.111 ± 0.064	0.117 ± 0.051	—
CoV k_3	28.724 ± 9.051	37.074 ± 6.578	—
k_4	0.047 ± 0.012	0.050 ± 0.019	—
CoV k_4	29.311 ± 15.001	34.342 ± 6.833	—
DV_{tot}	1.504 ± 0.774	3.614 ± 2.279	0.392 ± 0.104
CoV DV_{tot}	9.356 ± 5.439	15.987 ± 5.194	11.735 ± 10.435

CoV = coefficient of variation (%). K_1 (mL/(min × mg)) and k_2 – k_4 (1/min). Data are expressed as mean ± SD ($n = 4$).

Nearly 80% of lesions demonstrated uptake of ^{18}F -Galacto-RGD with high tumor-to-blood and tumor-to-muscle ratios. This corroborates previous findings that the integrin $\alpha_v\beta_3$ plays an essential role in aberrant angiogenesis, which is a hallmark of cancer and an indicator of poor prognosis (22). Tumor-induced angiogenesis is a multistep process involving a variety of different pro- and antiangiogenic factors and is often triggered by the release of growth factors and cytokines from hypoxic tumor cells. Neovascularization is required for adequate nutrition supply and, thus, important for tumor growth. Moreover, it also facilitates the metastatic spread into the blood circulation (23). It requires the interaction of endothelial cells with components of the

extracellular matrix during formation of new microvessels, which is mediated by endothelial integrins (24). It has been shown that $\alpha_v\beta_3$ is expressed on angiogenic blood vessels and on malignant tumors at elevated levels (25) and that a variety of $\alpha_v\beta_3$ integrin antagonists effectively prevents tumor metastasis, growth, and angiogenesis (26,27). Therefore, it is expected that many tumor lesions can be identified by an $\alpha_v\beta_3$ -selective tracer such as ^{18}F -Galacto-RGD. However, the intensity and pattern of uptake showed large inter- and intraindividual variations: In some patients, metastases and primary tumor demonstrated marked differences in tracer uptake (Fig. 7). In melanoma patients, there were large variations in tracer uptake observed between the pa-

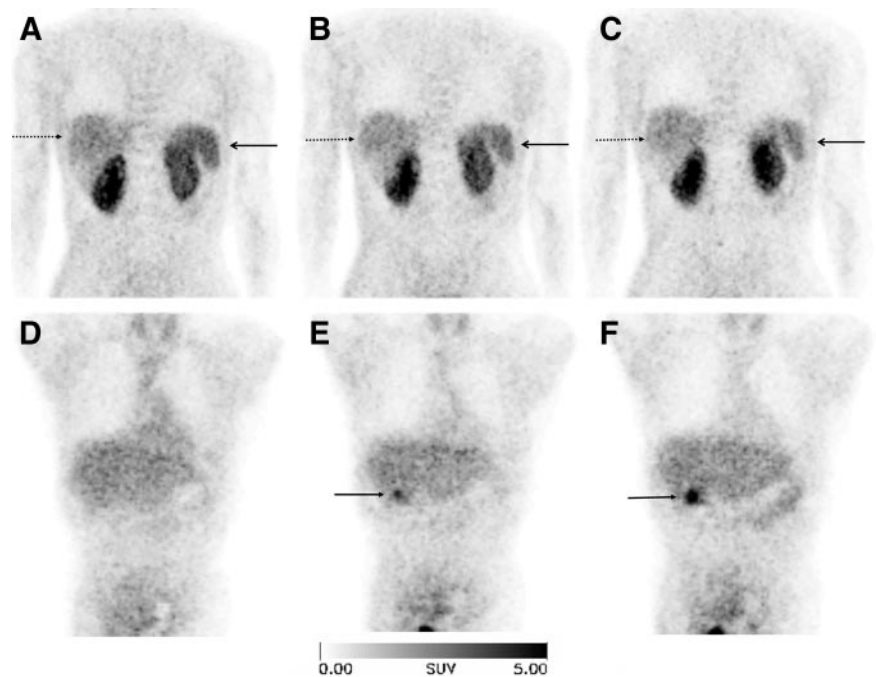


FIGURE 5. ^{18}F -Galacto-RGD scan of 56-year-old patient with multiple metastases to liver and intestine from malignant melanoma (patient 1). Static emission scans at 5, 30, and 60 min after injection (from left to right) with representative coronal views at level of kidneys (A–C) and at level of gallbladder (D–F). No lesions show tracer uptake, indicating lack of, or very low, $\alpha_v\beta_3$ expression. Liver (arrow with dotted line) shows moderate activity with only slow decrease over time, whereas spleen (open arrow tip) shows higher activity initially, decreasing over time. Gallbladder (closed arrow tip) shows increasing activity over time, indicating hepatobiliary excretion of tracer.

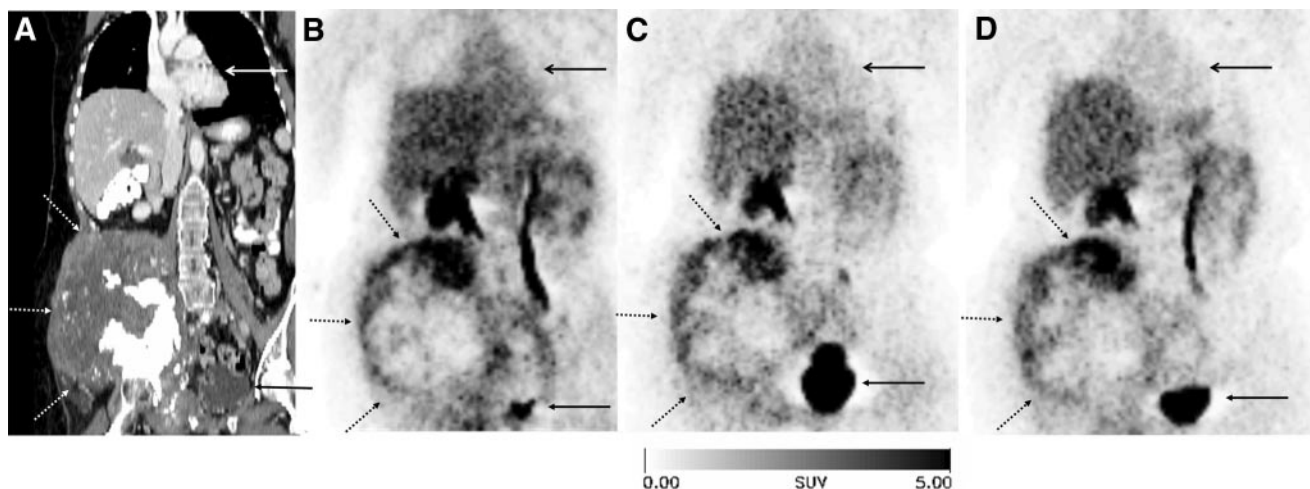


FIGURE 6. A 26-y-old patient (patient 9) with large chondrosarcoma of right pelvis (arrow with dotted line). Coronal reformation of CT scan (A) and corresponding coronal views of ^{18}F -Galacto-RGD scan (B–D) at 5, 40, and 90 min after injection (from left to right). Note rapid renal tracer excretion into bladder (closed arrow tip) and decrease of activity in blood pool (heart: open arrow tip). Tumor shows heterogeneous tracer uptake with focal maximum at top of tumor. Note there is only minimal decrease of activity over time. Patient had to void after second scan (C) and had to be repositioned for last scan (D); therefore, bladder is smaller in third scan compared with second scan.

tients (Fig. 8). These findings indicate great inter- and intraindividual diversity of $\alpha_v\beta_3$ expression in cancer patients, which is in accordance with the literature. For example, it is well established for human melanoma that the expression of $\alpha_v\beta_3$ plays an important role during the transition of cells from the radial growth phase to the vertical growth phase (28,29). However, further changes leading to metastases may be more complex and ultimately not dependent on $\alpha_v\beta_3$ expression or $\alpha_v\beta_3$ might be expressed in varying quantities during various stages of metastatic dissemination (30). Moreover, experiments in knockout mice lacking the integrin $\alpha_v\beta_3$ showed normal developmental angiogenesis and even excessive tumor angiogenesis, which led to a reevaluation of the role of $\alpha_v\beta_3$ in neovascularization (31). It seems that the absence of $\alpha_v\beta_3$ may be compensated by other vascular integrins or the vascular endothelial growth factor receptor 2 (VEGF R2), which are downregulated by $\alpha_v\beta_3$ (32,33). Therefore, it is currently assumed that $\alpha_v\beta_3$ bears a positive and a negative regulatory role in angiogenesis, depending on the respective biologic context. Therefore, noninvasive methods of determining the $\alpha_v\beta_3$ receptor status in humans, such as ^{18}F -Galacto-RGD PET, might be used to further elucidate the complex role of this integrin *in vivo*.

The kinetic modeling approach using the 2-TC model for tumors and the 1-TC model for muscle resulted in good parameter precision (CoV values) and good model fits to the data. Values for DV_{tot} were substantially higher in tumors and tumor maximum than in muscle, indicating increased free and bound tracer in tumor tissues compared with muscle. The good fit of the 2-TC model and the ratios of k_3/k_4 for tumors are indicative of specific and slowly reversible receptor binding of ^{18}F -Galacto-RGD. These results confirm

previously reported data on the properties of ^{18}F -Galacto-RGD and RGD peptides in general and their binding kinetics to the $\alpha_v\beta_3$ receptor (34). We showed that pretreatment with increasing concentrations of unlabeled $\alpha_v\beta_3$ antagonists before administration of ^{18}F -Galacto-RGD causes a concentration-dependent decrease of tracer accumulation in $\alpha_v\beta_3$ -positive tumors (10) and found an increasing tracer uptake with increasing $\alpha_v\beta_3$ expression in a murine tumor model, which strongly supports ^{18}F -Galacto-RGD binding specifically to $\alpha_v\beta_3$ (12). There are also reports indicating substantial internalization of labeled RGD peptides *in vitro* (35). However, the ability to estimate k_4 with good precision suggests that ^{18}F -Galacto-RGD is not irreversibly trapped inside the cells. However, because of several limitations of our modeling approach, these results have to be interpreted with care: First, only image-based arterial input functions were used; second, the first time frames of the dynamic studies were acquired for 30 s to achieve acceptable counting statistics. These factors probably lead to an underestimation of the peak plasma activity and consequently an overestimation of K_1 in our model. However, calculations with a lower estimated K_1 of 0.1, based on data obtained in solid tumors (19), resulted in similar DV_{tot} values compared with the K_1 derived from our modeling data. Moreover, recent studies on the kinetics of ^{18}F -FDG in tumors using image-based arterial input functions showed good model fits and revealed similar K_1 values compared with our results (36,37).

This new tracer offers a variety of possible applications. Recent data on ^{18}F -Galacto-RGD in a murine model of a delayed-type hypersensitivity reaction suggest that it is possible to assess $\alpha_v\beta_3$ expression in inflammatory processes. The authors conclude that ^{18}F -Galacto-RGD might be used

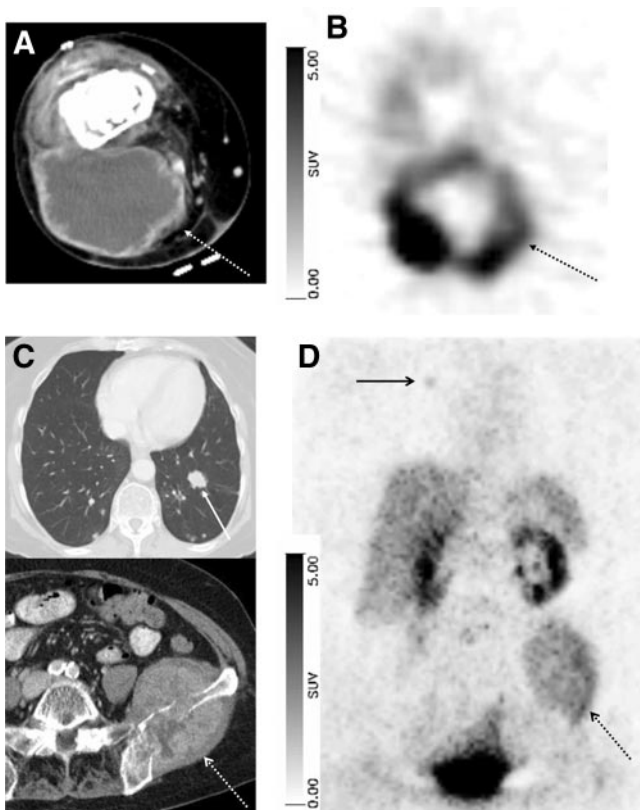


FIGURE 7. A 75-y-old female patient with soft-tissue sarcoma of distal right upper thigh and multiple metastases to bone and lungs. Primary tumor (arrow with dotted line) shows central necrosis and peripheral contrast enhancement in CT scan (A; transverse plane). ^{18}F -Galacto-RGD scan (B; transverse plane, 120 min after injection) shows intense peripheral tracer uptake (SUV, 10.0). A large osseous metastases in left iliac bone (arrow with open arrow tip and dotted line) shows only moderate tracer uptake (D; 90 min after injection; SUV, 2.7). Metastasis in left lower lobe of lung (arrow with closed arrow tip) shows no tracer uptake, whereas another metastasis in right upper lobe (arrow with open arrow tip) shows faint tracer uptake (SUV, 1.3). Corresponding contrast-enhanced CT scans at level of iliac bone and lower lobes of lungs are shown (C, transverse plane).

to distinguish between acute and chronic phases of T-cell-mediated immune response and to assess disease activity in autoimmune disorders (38). However, the fact that $\alpha_v\beta_3$ is also expressed on newly formed blood vessels in inflammatory processes poses some problems in the context of malignant diseases: First, the distinction between malignancies and inflammations might be impaired. Preliminary results in patients with pigmented villonodular synovitis suggest that the uptake of ^{18}F -Galacto-RGD in inflammatory lesions can be intense and similar to the uptake observed in malignancies (12). This might be a shortcoming of ^{18}F -Galacto-RGD, similar to ^{18}F -FDG, which can show high uptake in inflammatory cells (39).

Another potential clinical application would be to document $\alpha_v\beta_3$ expression of tumors before $\alpha_v\beta_3$ -directed therapies. This is of paramount importance for a correct interpretation of the results of clinical trials with corresponding $\alpha_v\beta_3$ antagonists, in which a substantial proportion of the patients' lesions might not be $\alpha_v\beta_3$ positive at all. No benefit can be expected in $\alpha_v\beta_3$ -negative lesions and the results of a trial concerning the effectiveness of $\alpha_v\beta_3$ antagonists would be false-negative. This is also illustrated by the results of our study, which showed large inter- and intraindividual variances of ^{18}F -Galacto-RGD accumulation. Furthermore, ^{18}F -Galacto-RGD might be used to assess the inhibition of the $\alpha_v\beta_3$ integrin, indicating whether the dose of $\alpha_v\beta_3$ antagonists might be optimized. Finally, $\alpha_v\beta_3$ expression has been reported to be an important factor in determining the invasiveness and malignant potential of tumors such as breast and colon cancer (40,41). Therefore, noninvasive quantification of $\alpha_v\beta_3$ expression may provide a unique method of characterizing the biologic aggressiveness of a malignant tumor in an individual patient without the need for collecting tissue samples.

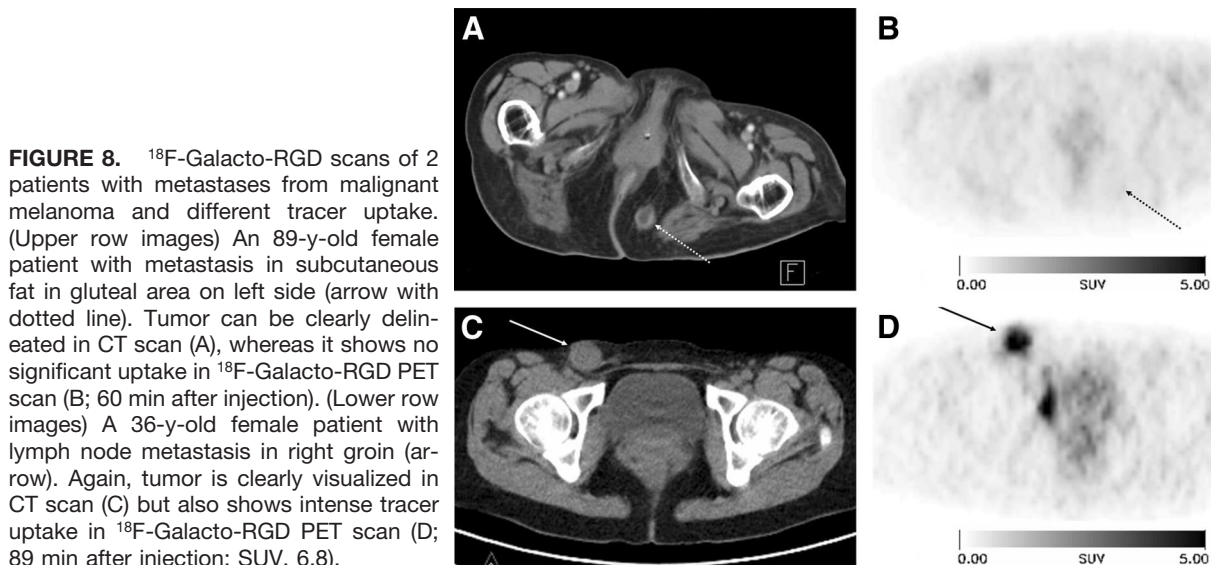


FIGURE 8. ^{18}F -Galacto-RGD scans of 2 patients with metastases from malignant melanoma and different tracer uptake. (Upper row images) An 89-y-old female patient with metastasis in subcutaneous fat in gluteal area on left side (arrow with dotted line). Tumor can be clearly delineated in CT scan (A), whereas it shows no significant uptake in ^{18}F -Galacto-RGD PET scan (B; 60 min after injection). (Lower row images) A 36-y-old female patient with lymph node metastasis in right groin (arrow). Again, tumor is clearly visualized in CT scan (C) but also shows intense tracer uptake in ^{18}F -Galacto-RGD PET scan (D; 89 min after injection; SUV, 6.8).

CONCLUSION

¹⁸F-Galacto-RGD is a tracer with highly desirable pharmacokinetic properties. The kinetic studies suggest specific binding of the tracer, which allows for noninvasive quantification of $\alpha_v\beta_3$ expression. Imaging of $\alpha_v\beta_3$ expression is possible with good contrast in most regions of the body except for the urogenital tract and, to a lesser extent, the spleen and liver. We recommend imaging ~60 min after injection of the tracer for optimal lesion-to-background contrast. By using furosemide to enhance diuresis, image quality adjacent to the bladder could be further improved.

ACKNOWLEDGMENTS

We thank Wolfgang Linke, Janette Carlsen, and the RDS-Cyclotron and PET team—especially Michael Herz, Gitti Dzewas, Coletta Kruschke, and Nicola Henke—for excellent technical assistance and the Münchner Medizinische Wochenschrift and the Sander-Foundation for financial support.

REFERENCES

- Cox D, Aoki T, Seki J, Motoyama Y, Yoshida K. The pharmacology of integrins. *Med Res Rev*. 1994;14:192–228.
- Hood JD, Cheresch DA. Role of integrins in cell invasion and migration. *Nat Rev Cancer*. 2002;2:91–100.
- Ruoslahti E. Specialization of tumor vasculature. *Nat Rev Cancer*. 2002;2:83–90.
- Brooks PC, Montgomery AM, Rosenfeld M, et al. Integrin $\alpha_v\beta_3$ antagonists promote tumor regression by inducing apoptosis of angiogenic blood vessels. *Cell*. 1994;79:1157–1164.
- Taga T, Suzuki A, Gonzalez-Gomez I, et al. Alpha-v integrin antagonist EMD 121974 induces apoptosis in brain tumor cells growing on vitronectin and tenascin. *Int J Cancer*. 2002;98:690–697.
- Dredge K, Dalglish AG, Marriott JB. Recent developments in antiangiogenic therapies. *Expert Opin Biol Ther*. 2002;2:953–966.
- Ruoslahti E, Pierschbacher MD. New perspectives in cell adhesion: RGD and integrins. *Science*. 1987;238:491–497.
- Haubner RH, Wester HJ, Weber WA, Schwaiger M. Radiotracer based strategies to image angiogenesis. *Q J Nucl Med*. 2003;47:189–199.
- Haubner R, Wester HJ, Reuning U, et al. Radiolabeled $\alpha_v\beta_3$ integrin antagonists: a new class of tracers for tumor targeting. *J Nucl Med*. 1999;40:1061–1071.
- Haubner R, Wester HJ, Weber WA, et al. Noninvasive imaging of $\alpha_v\beta_3$ integrin expression using ¹⁸F-labeled RGD-containing glycopeptide and positron emission tomography. *Cancer Res*. 2001;61:1781–1785.
- Haubner R, Kuhnast B, Mang C, et al. [¹⁸F]Galacto-RGD: synthesis, radiolabeling, metabolic stability and radiation dose estimates. *Bioconjug Chem*. 2004;15:61–69.
- Haubner R, Weber WA, Beer AJ, et al. Non-invasive visualization of the activated $\alpha_v\beta_3$ integrin in cancer patients by positron emission tomography and [¹⁸F]Galacto-RGD. *PLoS Med* [serial online]. March 2005;2(3):e70. Accessed May 19, 2005.
- Beer AJ, Haubner R, Essler M, et al. Non invasive imaging of $\alpha_v\beta_3$ expression with F-18-Galacto-RGD and PET: initial results in patients [abstract]. *J Nucl Med*. 2004;45(suppl):192P–193P.
- Nip J, Shibata H, Loskutoff DJ, Cheresch DA, Brodt P. Human melanoma cells derived from lymphatic metastases use integrin $\alpha_v\beta_3$ to adhere to lymph node vitronectin. *J Clin Invest*. 1992;90:1406–1413.
- Gutheil JC, Campbell TN, Pierce PR, et al. Targeted antiangiogenic therapy for cancer using vitaxin: a humanized monoclonal antibody to the integrin $\alpha_v\beta_3$. *Clin Cancer Res*. 2000;6:3056–3061.
- Patel SR, Jenkins J, Papadopoulos N, et al. Pilot study of vitaxin—an angiogenesis inhibitor—in patients with advanced leiomyosarcomas. *Cancer*. 2001;92:1347–1348.
- Weber WA, Ziegler SI, Thodtman R, Hanauske AR, Schwaiger M. Reproducibility of metabolic measurements in malignant tumors using FDG PET. *J Nucl Med*. 1999;40:1771–1777.
- Lodge MA, Lucas JD, Marsden PK, Cronin BF, O'Doherty MJ, Smith MA. A PET study of ¹⁸FDG uptake in soft tissue masses. *Eur J Nucl Med*. 1999;26:22–30.
- Tseng J, Dunnwald LK, Schubert EK, et al. ¹⁸F-FDG kinetics in locally advanced breast cancer: correlation with tumor blood flow and changes in response to neoadjuvant chemotherapy. *J Nucl Med*. 2004;45:1829–1837.
- Slifstein M, Laruelle M. Models and methods for derivation of in vivo neuroreceptor parameters with PET and SPECT reversible radiotracers. *Nucl Med Biol*. 2001;28:595–608.
- Spilker ME, Sprenger T, Valet M, et al. Quantification of [¹⁸F]diprenorphine kinetics in the human brain with compartmental and non-compartmental modeling approaches. *Neuroimage*. 2004;22:1523–1533.
- Fox SB, Gasparini G, Harris AL. Angiogenesis: pathological, prognostic and growth factor pathways and their link to trial design and anticancer drugs. *Lancet Oncol*. 2001;2:278–289.
- Fidler IJ. Angiogenesis and cancer metastasis. *Cancer J*. 2000;6:134–141.
- Eliceiri B, Cheresch DA. The role of α_v integrins during angiogenesis: insights into potential mechanisms of action and clinical development. *J Clin Invest*. 1999;103:1227–1230.
- Bello F, Francolini M, Marthyn P, et al. $\alpha_v\beta_3$ and $\alpha_v\beta_5$ integrin expression in glioma periphery. *Neurosurgery*. 2001;49:380–389.
- Haubner R, Finsinger D, Kessler H. Stereoisomeric peptide libraries and peptidomimetics for designing selective inhibitors of the $\alpha_v\beta_3$ integrin for a new cancer therapy. *Angew Chem Int Ed Engl*. 1997;36:1374–1389.
- Kerr JS, Slee AM, Mousa SA. The α_v integrin antagonists as novel anticancer agents: an update. *Expert Opin Investig Drugs*. 2002;11:1765–1774.
- McGary EC, Lev DC, Bar-Eli M. Cellular adhesion pathways and metastatic potential of human melanoma. *Cancer Biol Ther*. 2002;1:459–465.
- Johnson JP. Cell adhesion molecules in the development and progression of malignant melanoma. *Cancer Metastasis Rev*. 1999;18:345–357.
- Seftor RE, Seftor EA, Hendrix MJ. Molecular role(s) for integrins in human melanoma invasion. *Cancer Metastasis Rev*. 1999;18:359–375.
- Hynes RO. A reevaluation of integrins as regulators of angiogenesis. *Nat Med*. 2002;8:918–921.
- Blystone SD, Slater SJ, Williams SP, Crow MT, Brown EJ. A molecular mechanism of integrin crosstalk: $\alpha_v\beta_3$ suppression of calcium/calmodulin-dependent protein kinase II regulates $\alpha_5\beta_1$ function. *J Cell Biol*. 1999;145:889–897.
- Reynolds LE, Wyder L, Lively JC, et al. Enhanced pathological angiogenesis in mice lacking β_3 integrin or β_3 and β_5 integrin. *Nat Med*. 2003;8:27–34.
- Pfaff M, Tangemann K, Müller B, et al. Selective recognition of cyclic RGD peptides of NMR defined conformation by $\alpha_{IIb}\beta_3$, $\alpha_v\beta_3$, and $\alpha_5\beta_1$ integrins. *J Biol Chem*. 1994;269:20233–20238.
- Van Hagen PM, Breeman WAP, Bernard HF, et al. Evaluation of a radiolabelled cyclic DTPA-RGD analogue for tumour imaging and radionuclide therapy. *Int J Cancer*. 2000;90:186–198.
- Strauss LG, Dimitrakopoulou-Strauss A, Koczan D, et al. ¹⁸F-FDG kinetics and gene expression in giant cell tumors. *J Nucl Med*. 2004;45:1528–1535.
- Dimitrakopoulou-Strauss A, Strauss LG, Burger C, et al. Prognostic aspects of ¹⁸F-FDG PET kinetics in patients with metastatic colorectal carcinoma receiving FOLFOX chemotherapy. *J Nucl Med*. 2004;45:1480–1487.
- Pichler BJ, Kneilling M, Haubner R, et al. Imaging of delayed-type hypersensitivity reaction by PET and ¹⁸F-galacto-RGD. *J Nucl Med*. 2005;46:184–189.
- Kubota R, Yamada S, Kubota K, et al. Intratumoral distribution of fluorine-18-fluorodeoxyglucose in vivo: high accumulation in macrophages and granulation tissue studied by microautoradiography. *J Nucl Med*. 1992;33:1972–1980.
- Gasparini G, Brooks PC, Biganzoli E, et al. Vascular integrin $\alpha_v\beta_3$: a new prognostic indicator in breast cancer. *Clin Cancer Res*. 1998;4:2625–2634.
- Vonlaufen A, Wiedle G, Borisch B, Birrer S, Luder P, Imhof BA. Integrin $\alpha_v\beta_3$ expression in colon carcinoma correlates with survival. *Mod Pathol*. 2001;14:1126–1132.